

# FAR Planner: Fast, Attemptable Route Planner using Dynamic Visibility Update

Fan Yang, Chao Cao, Hongbiao Zhu, Jean Oh, and Ji Zhang

**Abstract**— We present our work on a fast route planner based on visibility graph. The method extracts edge points around obstacles in the environment to form polygons, with which, the method dynamically updates a global visibility graph, expanding the visibility graph along with the navigation and removing edges that become occluded by dynamic obstacles. When guiding a vehicle to the goal, the method can deal with both known and unknown environments. In the latter case, the method is attemptable in discovering a way to the goal by picking up the environment layout on the fly. We evaluate the method using both ground and aerial vehicles, in simulated and real-world settings. In highly convoluted unknown or partially known environments, our method is able to reduce travel time by 13-27% compared to RRT\*, RRT-Connect, A\*, and D\* Lite, and finds a path within 3ms in all of our experiments.

## I. INTRODUCTION

Visibility graph-based planning has been studied by the research society but has not gained substantial popularity. The main difficulties in visibility graph-based planning have to do with its requirement on a polygonal world and the limitation in extending to three-dimensional (3D) space. In this paper, we reconsider visibility graph in solving the path planning problem in the real world and demonstrate its strength in fast replanning and the ability to handle unknown and partially known environments. The main contribution of the paper is in dynamically building the visibility graph. The method finds the shortest path on the graph, if one exists, as other visibility graph-based methods [2].

Our method models obstacles in the environment as polygons. With data acquired from range sensors, the method extracts edge points around the obstacles and converts the edge points into a set of polygons. These polygons are merged over data frames and maintained at the global scale. When extending the method to 3D, we employ a multi-layer polygonal representation. Obviously, the finer the vertices and layers of the polygons are, the closer they approximate the real obstacles which can come in arbitrary shapes.

The method constantly updates a global visibility graph at every data frame. As the vehicle navigates, the method dynamically expands the visibility graph using a small amount of processing ( $\sim 20\%$  of a single i7 CPU thread). With the visibility graph dynamically updated, the method can search for a path at low latency (within 3ms). In the case that dynamic obstacles are present, the method eliminates edges on the visibility graph blocked by the dynamic obstacles and later on reconnects the edges after regaining the visibility.

All authors are with CMU Robotics Institute. Emails: {fanyang2, ccao1, hongbiaz, jeanoh, zhangji}@cmu.edu

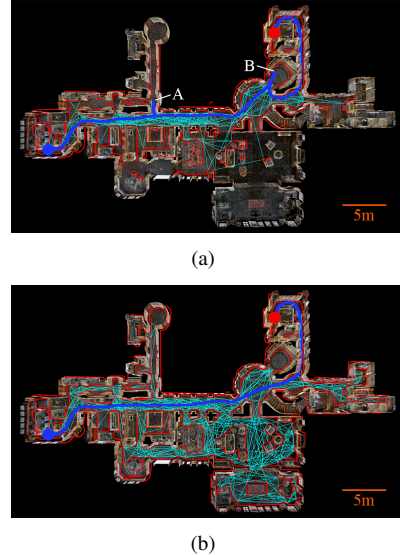


Fig. 1. Representative result in (a) unknown and (b) known environments using a Matterport3D [1] house model. The blue curve is the vehicle trajectory starting at the blue dot and ending at the red dot. In (a), the planner attempts to guide the vehicle to the goal by registering obstacles in the environment (red polygons) and building a visibility graph (cyan lines) along with the navigation. At A and B, it re-plans after discovering a better route. In (b), it uses the visibility graph from a prior map to plan the route.

Further, the planner is capable of dealing with both known and unknown environments. In a known environment, the paths are planned based on a prior map. In an unknown environment, however, multiple paths are attempted to guide the vehicle to the goal based on the environment layout observed along with the navigation process.

We evaluate the method using both ground and aerial vehicles, in simulated and real-world experiments. Our ground vehicle simulation experiments use a mid-scale, moderately convoluted indoor environment and a large-scale, highly convoluted tunnel-network environment. We use a physical robot in an environment including indoor and outdoor settings with dynamic obstacles present. In the moderately convoluted environment, our method improves the performance marginally compared to A\* [3] and D\* Lite [4]. In the highly convoluted environment, however, both methods are affected by excessive planning time. Our method reduces travel time by 13-27% compared to RRT\* [5], RRT-Connect [6], A\*, and D\* Lite. When compared to A\* and D\* Lite, our average search time is two orders of magnitude less.

The FAR Planner open-source software<sup>1</sup> has been integrated to our open-sourced Autonomous Exploration De-

<sup>1</sup>FAR Planner: [github.com/MichaelFYang/far\\_planner](https://github.com/MichaelFYang/far_planner)

velopment Environment<sup>2</sup> to promote research in navigation autonomy. The two repositories form a full stack of planning algorithms for ground vehicle navigation.

## II. RELATED WORK

The problem of path planning has been tackled from multiple angles. The approach described here is based on key results of random sampling-based, search-based, and learning-based planners, solving the planning problem in both known and unknown environments.

*Random sampling-based planners:* The classic methods in the Rapidly-expanding Random Tree (RRT) [7] family include the original RRT and its variances such as RRT\* [5], RRT-Connect [6], Informed RRT\* [8], and BIT\* [9]. Together with probabilistic roadmap-based (PRM) methods [10] such as Lazy PRM [11], these methods are designed to plan paths in known environments. In unknown or partially known environments, dynamic roadmap [12] and a number of extended [13]–[15] and hybrid [16] approaches have been developed. Overall, the methods have to frequently regenerate the random tree/graph to account for the newly observed environment, or considerably prune the random tree/graph from the last planning cycle to reuse it.

*Search-based planners:* These methods include Dijkstra's algorithm [17], A\* [3], D\* [18], and D\* Lite [4]. Dijkstra's algorithm and A\* search on a discretized grid. The methods often need a long replanning time due to they reinitialize the propagation at each planning cycle. The incremental versions of A\*, D\* and D\* Lite, are proposed to efficiently handle environment changes as well as navigate in unknown terrain. The methods reduce replanning time by reusing the results from the previous planning cycle and adjusting only the locally inconsistent states. However, more recent work [19], [20] discovers issues that when the vehicle reaches a dead-end and requires a distinctive path from the previous plan to leave the dead-end, the replanning time could become significant and even surpass the non-incremental A\*.

*Learning-based planners:* These methods [21]–[23] need to be trained by a baseline method or using ground-truth data. The training process essentially encodes map information in the internal representation, e.g., a deep network. During test time, the methods can handle environments sharing similar settings with the training environments. In essence, learning-based planners are data-driven and can be limited to the environments that are present in the training data.

This paper focuses on a metric-based method. The main contribution is a visibility graph-based planner capable of efficient replanning over long distances as well as dealing with unknown and partially known environments. Using visibility graph for robot navigation has been studied in the literature [2], [24]–[28], but it is not well applied in real-world applications and often requires well-defined obstacle geometry. Our work reconsiders visibility graph and benefits from the long and relative sparse visibility edges and dynamically adjusts them for attempting in unknown environments.

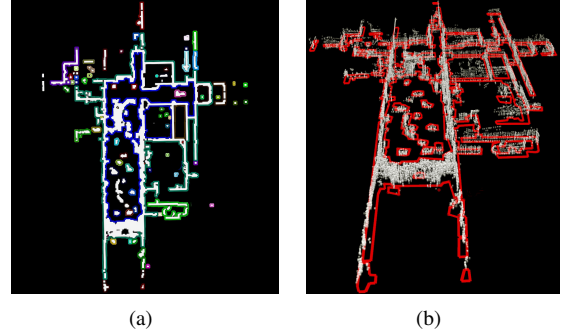


Fig. 2. (a) Polygons  $\{\mathcal{P}_{\text{contour}}^k\}$  extracted from blurred image  $\mathcal{I}_{\text{blur}}$  with dense vertices. The black pixels are traversable and the white pixels are obstacles. Different colors represent different polygons. (b) Final, extracted polygons  $\{\mathcal{P}_{\text{local}}^k\}$  (red) collated with sensor data points  $\mathcal{S}$  (white).

## III. METHODOLOGY

Define  $\mathcal{Q} \subset \mathbb{R}^3$  as the work space for the robot to navigate. Let  $\mathcal{S} \subset \mathcal{Q}$  be the set of sensor data points from obstacles. Our method develops a visibility graph (v-graph), denoted as  $\mathcal{G}$ , from  $\mathcal{S}$ . Given the robot position  $\mathbf{p}_{\text{robot}} \in \mathcal{Q}$  and goal  $\mathbf{p}_{\text{goal}} \in \mathcal{Q}$ , a path can be searched between  $\mathbf{p}_{\text{robot}}$  and  $\mathbf{p}_{\text{goal}}$ .

### A. Polygon Extraction

We describe the process of converting sensor data points  $\mathcal{S}$  into a set of polygons, denoted as  $\{\mathcal{P}_{\text{local}}^k \subset \mathcal{Q} \mid k \in \mathbb{Z}^+\}$ . For ground vehicles, very often, a terrain traversability analysis module runs in the system to analyze the terrain characteristics. The module takes in range measurements such as from Lidar or depth camera and outputs  $\mathcal{S}$  representing the obstacles. The polygon extraction process uses image processing techniques. Let  $\mathcal{I}$  be a binary image where a black pixel corresponds to a point in the traversable space and a white pixel corresponds to a point on an obstacle,  $\mathcal{I}$  is centered at the robot position  $\mathbf{p}_{\text{robot}}$ . We first project  $\mathcal{S}$  onto  $\mathcal{I}$  and at the same time inflate the points in  $\mathcal{S}$  using the vehicle size. Then, we blur the image with an average filter to create a grayscale image  $\mathcal{I}_{\text{blur}}$ . After that, we extract edge points in  $\mathcal{I}_{\text{blur}}$  and analyze the topological distribution of the edge points using the method in [29]. This gives us a set of enclosed polygons with dense vertices along the contour, as shown in Fig. 2. Denote the polygons as  $\{\mathcal{P}_{\text{contour}}^k \subset \mathcal{Q} \mid k \in \mathbb{Z}^+\}$ . For each  $\mathcal{P}_{\text{contour}}^k$ , we use the

---

### Algorithm 1: Polygon Extraction

---

**Input** : Sensor Data Points:  $\mathcal{S}$   
**Output:** Polygons:  $\{\mathcal{P}_{\text{local}}^k\}$   
1 Create binary image  $\mathcal{I}$  from points in  $\mathcal{S}$ ;  
2 Apply average filter to generate blurred image  $\mathcal{I}_{\text{blur}}$ ;  
3 Extract polygons  $\{\mathcal{P}_{\text{contour}}^k\}$  based on [29];  
4 **for** each  $\mathcal{P}_{\text{contour}}^k$  **do**  
5     Downsample vertices in  $\mathcal{P}_{\text{contour}}^k$  based on [30];  
6     Check the inner angle of each vertex and  
        eliminate the vertices with inner angle  $< \zeta$ ;  
7     Use vertices kept to form final polygon  $\mathcal{P}_{\text{local}}^k$ ;  
8 **end**

---

<sup>2</sup>Development Environment: [www.cmu-exploration.com](http://www.cmu-exploration.com)

method in [30] to downsize the vertices and further check the inner angle between the two connected edges on the contour for each vertex to infer the local curvature of the obstacle. The vertices with the inner angle less than a threshold are eliminated. The final, extracted polygons  $\{\mathcal{P}_{\text{local}}^k\}$  are shown in Fig. 1. To help readers follow the process, we write down the polygon extraction algorithm in Algorithm 1.

### B. Dynamic V-graph Update

The v-graph  $\mathcal{G}$  employed in this paper contains two layers – a local layer, denoted as  $\mathcal{L}_{\text{local}}$ , surrounding the robot and a global layer, denoted as  $\mathcal{L}_{\text{global}}$ , covering the observed environment. At each data frame,  $\mathcal{L}_{\text{local}}$  is generated from sensor data points  $\mathcal{S}$  and then merged with  $\mathcal{L}_{\text{global}}$ . We know that the computational complexity of constructing a v-graph is  $O(n^2 \log n)$  [31], where  $n$  is the number of vertices on the v-graph. Given that our v-graph is constructed locally on  $\mathcal{L}_{\text{local}}$ , the computational cost is considerably limited. In other words, our method incrementally updates the v-graph to distribute the computation evenly to every data frame by updating only the area in the vicinity of the vehicle.

*Constructing Local Layer:* Recall that the sensor data points  $\mathcal{S}$  are converted into polygons  $\{\mathcal{P}_{\text{local}}^k\}$ . With  $\{\mathcal{P}_{\text{local}}^k\}$ , we construct a partially reduced v-graph on the local layer  $\mathcal{L}_{\text{local}}$ . Let  $\mathcal{E}_{\text{local}}$  be the set of visibility edges on  $\mathcal{L}_{\text{local}}$ . Specifically, for the edges in  $\mathcal{E}_{\text{local}}$  that are longer than a threshold, we neglect the unnecessary edges that head into the one or both connected polygons and keep the edges that “pass around” (see Fig. 3). The edges in  $\mathcal{E}_{\text{local}}$  that are shorter than the threshold are all kept without “reduction”. This is due to the effect of position noises of the vertices in  $\mathcal{E}_{\text{local}}$  is increased with shorter edges, causing larger direction changes of the edges and making it hard to identify whether the edges are heading into the polygon or not. Specifically, the edges that form the polygons in  $\{\mathcal{P}_{\text{local}}^k\}$  are also kept in  $\mathcal{E}_{\text{local}}$  as they “pass around” the polygons. In practice, we observe that the traversable space in an environment is often constrained where majority of the visibility edges are blocked by polygons close by, resulting in a relatively small number of final, connected edges in  $\mathcal{E}_{\text{local}}$ .

*Updating Global Layer:* After constructing the local v-graph on  $\mathcal{L}_{\text{local}}$ , we merge  $\mathcal{L}_{\text{local}}$  with  $\mathcal{L}_{\text{global}}$  to update  $\mathcal{L}_{\text{global}}$  in the area overlapping with  $\mathcal{L}_{\text{local}}$ . Define  $\{\mathcal{P}_{\text{global}}^l \subset \mathcal{Q} \mid l \in \mathbb{Z}^+\}$  as the set of polygons and  $\mathcal{E}_{\text{global}}$  as the set of visibility edges on  $\mathcal{L}_{\text{global}}$ . The process starts with associating the vertices between  $\{\mathcal{P}_{\text{local}}^k\}$  and  $\{\mathcal{P}_{\text{global}}^l\}$ . A vertex in  $\{\mathcal{P}_{\text{local}}^k\}$  is associated to the vertex in  $\{\mathcal{P}_{\text{global}}^l\}$  only if they are the closest vertex to each other and the

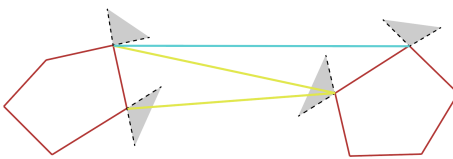


Fig. 3. Illustration of reduced v-graph. The two red polygons represent  $\{\mathcal{P}_{\text{local}}^k\}$ . Visibility edges (yellow) that head into one or both connected polygons from the shaded angles are useless and eliminated, and edges (cyan) that “pass around” the polygons are kept.

euclidean distance in between is less than a threshold. Then, for the vertices in  $\{\mathcal{P}_{\text{global}}^l\}$  that are associated, the positions are updated. Here, we use robust fitting [32] to further eliminate outlier associations. Given a vertex in  $\{\mathcal{P}_{\text{global}}^l\}$ , the corresponding vertices over a number of data frames are filtered through an iteration process. The iterations start with all the vertices as inliers. At each iteration, we re-calculate the mean and covariance of the inliers and use those to re-assign the inliers and outliers among the vertices. The iterations terminate if the inliers stay the same over two consecutive iterations or a maximum iteration number is met. Then, the vertex in  $\{\mathcal{P}_{\text{global}}^l\}$  is updated to the mean of the inliers. For the vertices in  $\{\mathcal{P}_{\text{global}}^l\}$  that are not associated, they are removed based on a voting result where an association is not found for certain times over a number of data frames. For the vertices in  $\{\mathcal{P}_{\text{local}}^k\}$  that are not associated, they are added to  $\{\mathcal{P}_{\text{global}}^l\}$  as new vertices. Finally, the edges in  $\mathcal{E}_{\text{local}}$  are merged into  $\mathcal{E}_{\text{global}}$ . If the edges exist in  $\mathcal{E}_{\text{global}}$ , they are updated, otherwise they are added as new edges. The overall process of the v-graph update is presented in Algorithm 2.

### C. Planning on V-Graph

Given the robot position  $\mathbf{p}_{\text{robot}}$  and goal  $\mathbf{p}_{\text{goal}}$ , we would like to search the v-graph  $\mathcal{G}$  for the shortest path between  $\mathbf{p}_{\text{robot}}$  and  $\mathbf{p}_{\text{goal}}$ . We first add  $\mathbf{p}_{\text{robot}}$  and  $\mathbf{p}_{\text{goal}}$  as two vertices on the global layer  $\mathcal{L}_{\text{global}}$  and connect them to the vertices in  $\{\mathcal{P}_{\text{global}}^l\}$  with non-blocking visibility edges. Then, a breath-first search is run on  $\mathcal{L}_{\text{global}}$  to propagate through  $\mathcal{E}_{\text{global}}$  and find the shortest path between  $\mathbf{p}_{\text{robot}}$  and  $\mathbf{p}_{\text{goal}}$ , if a path is available. Otherwise, the search reports no path found. The path search runs on a separate CPU thread and can produce the result at low latency.

---

#### Algorithm 2: Dynamic V-graph Update

---

```

Input : Sensor Data:  $\mathcal{S}$ , V-graph:  $\mathcal{G}$ 
Output: Updated v-graph  $\mathcal{G}$ 
1  $\{\mathcal{P}_{\text{vertex}}^k\} \leftarrow \text{PolygonExtraction}(\mathcal{S});$ 
2 Construct partially reduced v-graph on  $\mathcal{L}_{\text{local}}$ ;
3 Associate vertices between  $\{\mathcal{P}_{\text{local}}^k\}$  and  $\{\mathcal{P}_{\text{global}}^l\}$ ;
4 for each vertex  $\in \{\mathcal{P}_{\text{local}}^k\} \cup \{\mathcal{P}_{\text{global}}^l\}$  do
5   if an association exists then
6     | Update the vertex in  $\{\mathcal{P}_{\text{global}}^l\}$  to the mean of
      | the inliers assigned by robust fitting;
7   end
8   else if the vertex  $\in \{\mathcal{P}_{\text{global}}^l\}$  then
9     | Remove the vertex from  $\{\mathcal{P}_{\text{global}}^l\}$  based on
      | voting result;
10  end
11  else
12    | Add the vertex to  $\{\mathcal{P}_{\text{global}}^l\}$  as a new vertex;
13  end
14 end
15 Merge edges from  $\mathcal{E}_{\text{local}}$  into in  $\mathcal{E}_{\text{global}}$  and eliminate
   | those blocked or connected with removed vertices;

```

---

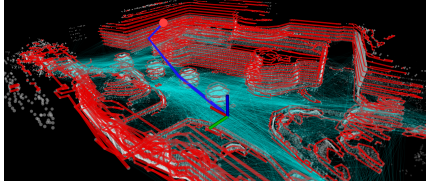


Fig. 4. Example 3D v-graph. Multi-Layer polygons (red) are extracted from a 3D environment. The visibility edges (cyan lines) cross multiple polygon layers. Further, a path (blue) is searched on the 3D v-graph between the robot position (coordinate frame) and goal (red dot).

As the robot navigates through the environment, the vertices in  $\{\mathcal{P}_{\text{global}}^l\}$  that have established non-blocking visibility edges with  $\mathbf{p}_{\text{robot}}$  form the free space, and the rest vertices in  $\{\mathcal{P}_{\text{global}}^l\}$  form the unknown space. After the navigation completes, the v-graph is saved with a label associated with each vertex to indicate the type of space. For future runs, the v-graph can be loaded into the planner as a prior map. When searching for a path through the vertices, we have the option of searching in the combined space or free space only. The first option is suitable for planning in unknown environments such as in Fig. 1(a) where the goal is located in unknown space. The second option is suitable for planning in known environments such as in Fig. 1(b).

#### D. Extension to 3D

The 3D version of our method models the environment as multiple horizontal slices and extracts multi-layer polygons. The visibility edges are connected across multiple polygon layers. Note that the partially reduced v-graph only applies to the visibility edges on a single polygon layer. For the visibility edges that connect different polygon layers, we keep all the non-blocking edges. Also, for the visibility edge that crosses three or more polygon layers, the collision check takes into account the blockage of the polygons on a mid-layer that the edge passes through. An example 3D v-graph and a path searched on the v-graph are shown in Fig. 4.

## IV. EXPERIMENTS

Our ground vehicle platform and simulated aerial vehicle platform are shown in Fig. 5. Both vehicles are equipped with a Velodyne Puck Lidar used as the range sensor for navigation planning. The ground vehicle has a camera at  $640 \times 360$  resolution and a MEMS-based IMU, coupled with the Lidar for state estimation [33]. The onboard autonomy system incorporates navigation modules from our development environment, e.g., collision avoidance, terrain analysis, and way-point following as fundamental navigation modules, and runs FAR planner on the top.

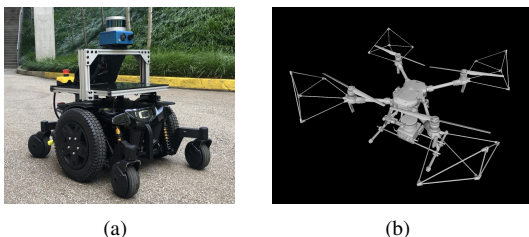


Fig. 5. (a) Ground experiment and (b) Simulated aerial platforms.

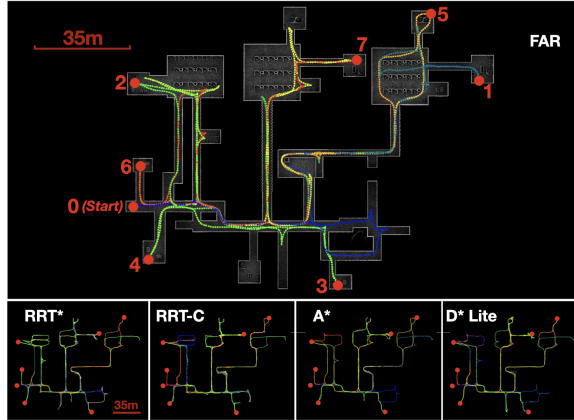
In all experiments, FAR planner runs on a 4.1GHz i7 computer. We configure FAR planner to update the v-graph at 2.5Hz and conduct a path search for replanning after each v-graph update. The planner uses images at 0.2m/pixel resolution to extract edge points and form polygons. The local layer on the v-graph is in a  $40\text{m} \times 40\text{m}$  area with the vehicle in the center. The threshold for the length of the visibility edge to use reduced v-graph is set to 5m.

#### A. Ground Vehicle Simulation

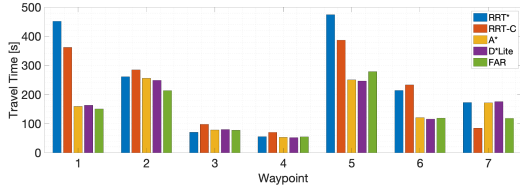
These experiments use the same vehicle and sensor configurations as our real ground vehicle platform in Fig. 5(a). The speed is set to 2m/s. We use a mid-scale, moderately convoluted indoor environment and a large-scale, highly convoluted tunnel-network environment. Fig. 6 and Fig. 7 show the results from the indoor environment and tunnel-network environment, respectively. For both environments, we set the vehicle to navigate through a series of points. The experiment includes two settings. In the *unknown* environment setting, we reset the planner after the vehicle arrives at each point, such that the environment becomes unknown as the vehicle navigates toward the next point in the series. In the *partially known* environment setting, we do not reset the planner but let it accumulate the environment observations through the entire run, i.e., as the vehicle navigates through the environment, the environment gradually becomes a partially known environment.

In Fig. 6(a) and Fig. 7(a), we show the trajectories from the run with planner reset where FAR planner produces efficient trajectories. RRT\*, RRT-Connect are prone to randomness and often generate back-and-forth patterns along the trajectories. Further, RRT\*, A\*, and D\* Lite suffer from long replanning time especially when the vehicle reaches a dead-end. Fig. 6(b)-(c) and Fig. 7(b)-(c) present the travel time to each point and the search time with planner reset. Fig. 6(d)-(e) and Fig. 7(d)-(e) show the same metrics with accumulated environment observations.

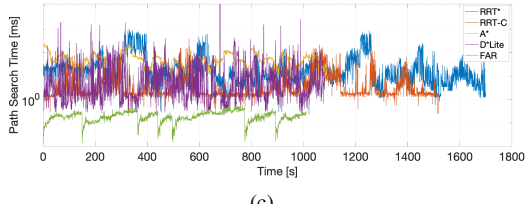
In Table I and Table II, we give the overall travel time and average search time through the entire runs. The numbers in Table I indicates that in the indoor environment with a moderate degree of convolution, FAR planner takes 7% less time than A\* and 6% less time than D\* Lite in finishing the run, while in the tunnel-network environment with a high degree of convolution, FAR planner finishes the run 27% faster than RRT\*, 21% faster than RRT-Connect, 13% faster than A\*, and 27% faster than D\* Lite. The average search time of A\* in the tunnel-network environment is 400.1ms and 417.0ms for the two runs as shown in Table II. Note that A\* is known for its resolution completeness in finding the optimal path. However, it is affected by a long search time causing slow responses to the newly observed environment. For instance, when new obstacles show up in front of the vehicle, the planner is not able to update the path in time. The vehicle frequently stops waiting for an updated path. The average search time of D\* Lite, which is designed to handle such dynamic changes, is 138.3ms and 89.1ms, respectively. D\* Lite's processing is lightweight when the



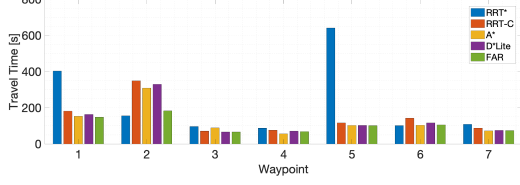
(a)



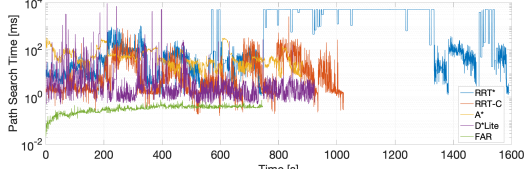
(b)



(c)



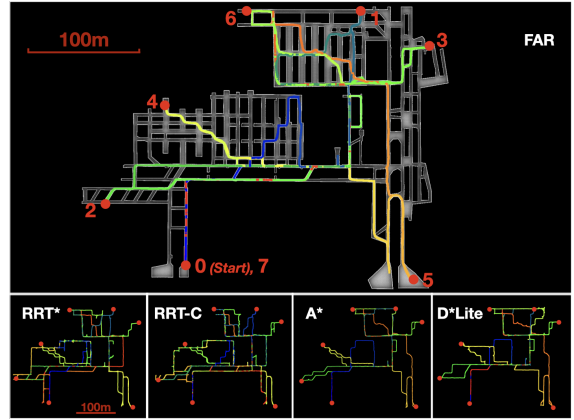
(d)



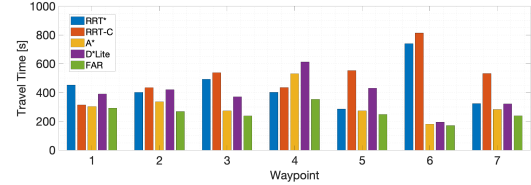
(e)

Fig. 6. Ground vehicle simulation in mid-scale, moderately convoluted indoor environment. The vehicle is set to navigate in increasing order from the start (point 0) to point 7 (see labels in (a)). The experiment is conducted in two runs. In the first run, the planner is reset after arriving at each point. This mimics navigation in an unknown environment. In the second run, the planner accumulates the environment observations through the run. This mimics navigation in a partially known environment. The trajectories in (a) are from the run with planner reset. (b) and (c) present the time of arrival at each point and the search time with planner reset. (d) and (e) show the same metrics with accumulated environment observations. In this moderately convoluted environment, FAR planner reduces the travel time marginally in comparison to A\* and D\* Lite. The search time of FAR planner is significantly less than all the other planners.

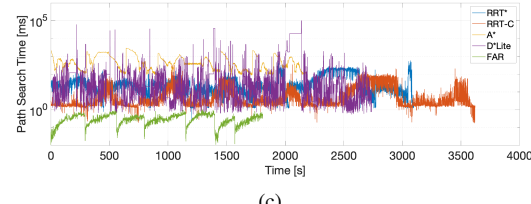
newly observed environment changes only a small number of states. However, when the vehicle reaches a dead-end, many states become inconsistent and the replanning takes a large number of iterations for the states to converge to



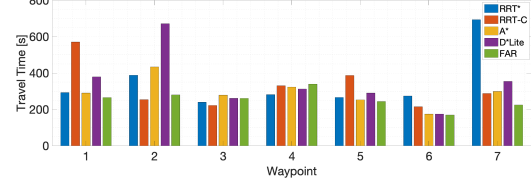
(a)



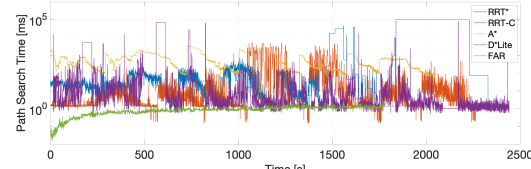
(b)



(c)



(d)



(e)

Fig. 7. Ground vehicle simulation in large-scale, highly convoluted tunnel-network environment. The figure shares the same layout with Fig. 6. FAR planner reduces the travel time substantially in comparison to RRT\*, RRT-Connect, A\*, and D\* Lite. Same as Fig. 6, the search time of FAR planner is significantly less than all the other planners.

consistency. FAR Planner achieves an average search time of 0.38 and 0.88, respectively, using a separate thread running in the background to update the v-graph. For the experiments in Fig. 6 and Fig. 7, the v-graph update consumes between 14-63ms and runs at 2.5Hz. In comparison, RRT\*, RRT-Connect, A\*, and D\* Lite update the random tree/grid states during the propagation. Given the nature of these methods, the two tasks are hard to separate. The time spent on finding a path takes into account the processing on both tasks.

TABLE I

OVERALL TRAVEL TIME IN [S] FOR GROUND VEHICLE SIMULATION

Test	RRT*	RRT-connect	A*	D* Lite	FAR
Indoor (reset)	1700	1519	1090	1082	<b>1012</b>
Indoor (accumulate)	1593	1024	883	924	<b>746</b>
Tunnel (reset)	3097	3620	2180	2740	<b>1809</b>
Tunnel (accumulate)	2434	2263	2051	2442	<b>1781</b>

TABLE II

AVERAGE SEARCH TIME IN [MS] FOR GROUND VEHICLE SIMULATION

Test	RRT*	RRT-Connect	A*	D* Lite	FAR
Indoor (reset)	40.6	7.1	60.0	29.0	<b>0.20</b>
Indoor (accumulate)	329.5	25.4	59.2	26.5	<b>0.33</b>
Tunnel (reset)	39.9	10.7	400.1	138.3	<b>0.38</b>
Tunnel (accumulate)	258.4	49.1	417.0	89.1	<b>0.88</b>

### B. Ground Vehicle Physical Experiment

The physical experiment uses the ground vehicle platform in Fig. 5(a) with the speed set to 1.5m/s. As shown in Fig. 8, the vehicle starts from the inside of a building, navigates to the outside, and reaches goal in a garage building. The environment is unknown. The vehicle gets into four dead-ends and then re-routes. A cart initially blocks the vehicle path forcing it to choose another way that leads to a dead-end. While the vehicle navigates out of the dead-end, the cart is removed allowing the vehicle to pass through. In an outdoor area, pedestrians are present as dynamic obstacles. FAR planner disconnects the visibility edges blocked by the pedestrians and later on reconnects them after the pedestrians

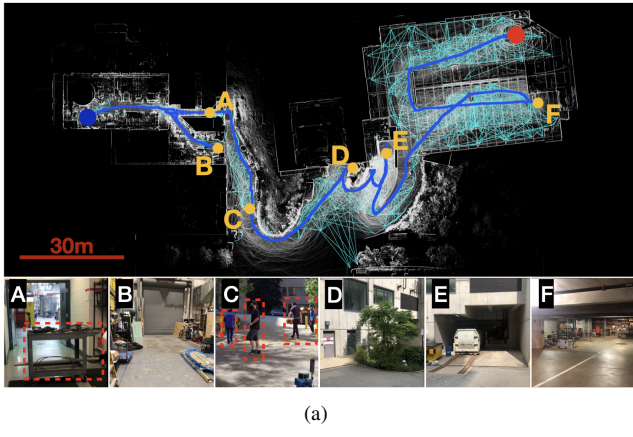


Fig. 8. Ground vehicle physical experiment. In (a), the blue curve is the vehicle trajectory starting at the blue dot and ending at the red dot. The vehicle starts from the inside of a building, navigates to the outside, and reaches goal in a garage building. The environment is unknown. The visibility edges (cyan) are developed during the navigation. The small images on the bottom are taken from A to F as labeled on the trajectory. B, D, E, and F are four dead-ends where the vehicle re-routes. At A, a cart in a corridor blocks the path forcing the vehicle to choose another way and get into a dead-end at B. On the way back, the cart is removed and the vehicle navigates through the corridor to the outside. The area around C involves dynamic obstacles. (b) shows the search time through the run.

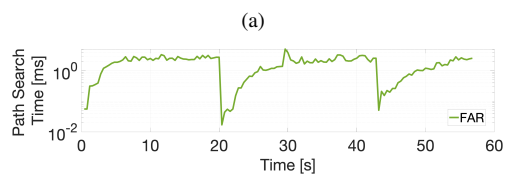
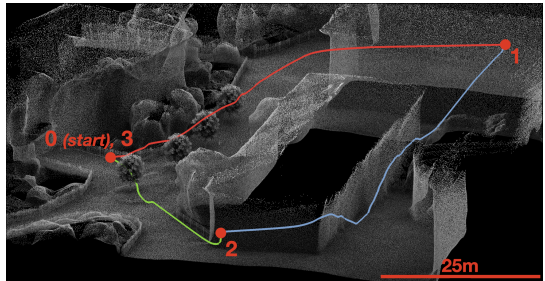


Fig. 9. Aerial vehicle simulation in campus environment. Similar to the ground vehicle simulation experiments, the vehicle is set to navigate in increasing order from the start to point 3 (see labels in (a)). The planner is reset after the vehicle arrives at each point. (b) presents the search time.

move away. Fig. 9(b) presents the search time through the run. The vehicle drives 388m in 406s.

FAR planner is used by the CMU-OSU team as the main route planner in attending DARPA Subterranean Challenge. In the final competition, the team received a “Most Sectors Explored Award” by conducting the most complete traversing and mapping across the site (26 out of 28 sectors).

### C. Aerial Vehicle Simulation

We use the simulated aerial platform in Fig. 5(b) with the speed set to 4m/s. The 3D version of FAR planner uses multi-layer polygons. The vertical distance between the polygon layers is 1m. The visibility edges connect across four polygon layers. Fig. 9 shows a preliminary result in simulation using an environment based on the university campus. The vehicle follows a series of points and navigates as in an unknown environment. Fig. 9(a) presents the trajectory and Fig. 9(b) shows the search time through the run. Overall, the vehicle flies through a 210m trajectory in 57s.

## V. CONCLUSION

We present a path planning method based on visibility graph. The method is capable of efficiently handling unknown and partially known environments. The method uses a two-layer implementation of the visibility graph, constructing the local layer in the vicinity of the vehicle at each data frame and merging the local layer into the global layer for visibility graph update. The path search is conducted by propagating through the visibility graph on an independent CPU thread, which finds paths at low latency. We evaluate the method in both simulated and real-world environments, with ground and aerial vehicles. The results indicate that in highly convoluted environments, our method substantially reduces the travel time and uses significantly less search time compared to state-of-the-art methods.

## REFERENCES

- [1] A. Chang, A. Dai, T. Funkhouser, M. Halber, M. Niessner, M. Savva, S. Song, A. Zeng, and Y. Zhang, "Matterport3D: Learning from RGB-D data in indoor environments," *International Conference on 3D Vision (3DV)*, 2017.
- [2] T. Lozano-Pérez and M. A. Wesley, "An algorithm for planning collision-free paths among polyhedral obstacles," *Communications of the ACM*, vol. 22, no. 10, p. 560–570, 1979.
- [3] P. Hart, N. Nilsson, and B. Raphael, "A formal basis for the heuristic determination of minimum cost paths," *IEEE Transactions on Systems Science and Cybernetics*, vol. 4, no. 2, pp. 100–107, 1968.
- [4] S. Koenig and M. Likhachev, "Fast replanning for navigation in unknown terrain," *IEEE Transactions on Robotics*, vol. 21, no. 3, pp. 354–363, 2005.
- [5] S. Karaman and E. Frazzoli, "Sampling-based algorithms for optimal motion planning," *The International Journal of Robotics Research*, vol. 30, no. 7, pp. 846–894, 2011.
- [6] J. Kuffner and S. LaValle, "RRT-connect: An efficient approach to single-query path planning," in *IEEE International Conference on Robotics and Automation*, 2000, pp. 995–1001.
- [7] S. M. LaValle, J. J. Kuffner, B. Donald *et al.*, "Rapidly-exploring random trees: Progress and prospects," *Algorithmic and computational robotics: new directions*, vol. 5, pp. 293–308, 2001.
- [8] J. D. Gammell, S. S. Srinivasa, and T. D. Barfoot, "Informed RRT\*: Optimal sampling-based path planning focused via direct sampling of an admissible ellipsoidal heuristic," in *IEEE/RSJ International Conference on Intelligent Robots and Systems*, 2014, pp. 2997–3004.
- [9] J. Gammell, S. Srinivasa, and T. Barfoot, "Batch Informed Trees (BIT\*): Sampling-based optimal planning via the heuristically guided search of implicit random geometric graphs," in *IEEE International Conference on Robotics and Automation*, 06 2015, pp. 3067–3074.
- [10] L. Kavraki, P. Svestka, J.-C. Latombe, and M. Overmars, "Probabilistic roadmaps for path planning in high-dimensional configuration spaces," *IEEE Transactions on Robotics and Automation*, vol. 12, no. 4, pp. 566–580, 1996.
- [11] R. Bohlin and L. Kavraki, "Path planning using lazy PRM," in *IEEE International Conference on Robotics and Automation*, 2000, pp. 521–528.
- [12] M. Kallman and M. Mataric, "Motion planning using dynamic roadmaps," in *IEEE International Conference on Robotics and Automation*, 2004, pp. 4399–4404.
- [13] Y. Tian, L. Yan, G.-Y. Park, S.-H. Yang, Y.-S. Kim, S.-R. Lee, and C.-Y. Lee, "Application of RRT-based local path planning algorithm in unknown environment," in *International Symposium on Computational Intelligence in Robotics and Automation*, 2007, pp. 456–460.
- [14] C. Lanzoni, A. Sanchez, and R. Zapata, "Sensor-based motion planning for car-like mobile robots in unknown environments," in *IEEE International Conference on Robotics and Automation*, 2003, pp. 4258–4263.
- [15] D. Ferguson, N. Kalra, and A. Stentz, "Replanning with RRTs," in *IEEE International Conference on Robotics and Automation*, 2006, pp. 1243–1248.
- [16] R. Fisher, B. Rosman, and V. Ivan, "Real-time motion planning in changing environments using topology-based encoding of past knowledge," in *IEEE/RSJ International Conference on Intelligent Robots and Systems*, 2018, pp. 6512–6517.
- [17] E. W. Dijkstra, "A note on two problems in connexion with graphs," *Numerische mathematik*, vol. 1, no. 1, pp. 269–271, 1959.
- [18] A. Stentz, "Optimal and efficient path planning for partially known environments," in *Intelligent Unmanned Ground Vehicles*, 1997, pp. 203–220.
- [19] A. T. Le, M. Q. Bui, T. D. Le, and N. Peter, "D\* Lite with reset: Improved version of D\* Lite for complex environment," in *IEEE International Conference on Robotic Computing*, 2017, pp. 160–163.
- [20] S. C. Yun, V. Ganapathy, and T. W. Chien, "Enhanced D\* Lite algorithm for mobile robot navigation," in *IEEE Symposium on Industrial Electronics and Applications*, 2010, pp. 545–550.
- [21] C. Richter and N. Roy, *Bayesian Learning for Safe High-Speed Navigation in Unknown Environments*, 01 2018, pp. 325–341.
- [22] J. Zeng, R. Ju, L. Qin, Y. Hu, Q. Yin, and C. Hu, "Navigation in unknown dynamic environments based on deep reinforcement learning," *Sensors*, vol. 19, p. 3837, 09 2019.
- [23] X. Guo and Y. Fang, "Learning to navigate in unknown environments based on GMRP-N," in *IEEE Annual International Conference on CYBER Technology in Automation, Control, and Intelligent Systems*, 2019, pp. 1453–1458.
- [24] B. Oommen, S. Iyengar, N. Rao, and R. Kashyap, "Robot navigation in unknown terrains using learned visibility graphs. Part I: The disjoint convex obstacle case," *IEEE Journal on Robotics and Automation*, vol. 3, no. 6, pp. 672–681, 1987.
- [25] N. Rao, "Robot navigation in unknown generalized polygonal terrains using vision sensors," *IEEE Transactions on Systems, Man, and Cybernetics*, vol. 25, no. 6, pp. 947–962, 1995.
- [26] D. Wooden and M. Egerstedt, "Oriented visibility graphs: low-complexity planning in real-time environments," in *Proceedings 2006 IEEE International Conference on Robotics and Automation, 2006. ICRA 2006.*, 2006, pp. 2354–2359.
- [27] H. Kaluder, M. Brezak, and I. Petrovic, "A visibility graph based method for path planning in dynamic environments," in *The 34th International Convention MIPRO*, 2011, pp. 717–721.
- [28] M. El Khaili, "Visibility graph for path planning in the presence of moving obstacles," *Engineering Science and Technology an International Journal*, vol. 4, pp. 118–123, 09 2014.
- [29] S. Suzuki and K. Abe, "Topological structural analysis of digitized binary images by border following," *Computer Vision, Graphics, and Image Processing*, vol. 30, pp. 32–46, 1985.
- [30] C.-H. Teh and R. Chin, "On the detection of dominant points on digital curves," *IEEE Transactions on Pattern Analysis and Machine Intelligence*, vol. 11, no. 8, pp. 859–872, 1989.
- [31] D.-T. Lee, "Proximity and reachability in the plane." Ph.D. dissertation, USA, 1978.
- [32] R. Andersen and S. Publications, *Modern Methods for Robust Regression*. SAGE Publications, 2008.
- [33] J. Zhang and S. Singh, "Laser-visual-inertial odometry and mapping with high robustness and low drift," *Journal of Field Robotics*, vol. 35, no. 8, pp. 1242–1264, 2018.